Effect of Covalent Modification on Proton-Coupled Electron Transfer at Quinone-Functionalized Carbon Electrodes

Fiki V. Owhoso¹, Sanat V. Modak², Partha Saha², *David G. Kwabi²

¹Department of Chemical Engineering, ²Department of Mechanical Engineering

University of Michigan, Ann Arbor, 2350 Hayward St, Ann Arbor, Michigan, 48109, United States

Abstract

The attachment of molecular species to conductive carbon electrodes is attracting attention as one strategy for developing high-performance functional materials for a large variety of electrochemical energy storage and conversion applications. It is critical to the optimal design of these materials that there is a fundamental understanding of how these functionalized molecular species interact with the electrical double layer at the electrode electrolyte interface. In this work, we investigate the aqueous electrochemical behavior of glassy carbon electrodes that were functionalized with 1-aminoanthraquinone-2-sulfonic acid (AAQS) via two conjugation techniques: amide coupling and radical-mediated diazonium reduction. The two conjugation routes gave rise to electrodes with distinct redox potential vs pH (i.e., Pourbaix) slopes, suggestive of distinct proton-coupled electron transfer (PCET) energetics. We relate measured Pourbaix slope to the electrostatic potential drop experienced by the quinone. Additionally, using a simple multilayer dielectric model of the double layer, we show how differing PCET energetics as a function of AAQS conjugation mode and electrolyte concentration can be explained in large part by differing distances between the ketone moiety in each quinone and the electrode, and thus differing driving forces for interfacial electric field-driven protonation of each quinone. Our results highlight the potential for the use of PCET thermochemistry to map out the electric field/electrostatic potential profile at electrode|electrolyte interfaces which is of relevance to many emerging electrochemical technologies.

Keywords: quinone, electrical double layer, covalent conjugation, proton-coupled electron transfer (PCET)

Introduction

Electrodes functionalized with molecularly well-defined reactive/catalytic species have become attractive for promoting a wide variety of electrochemical energy conversion processes or systems, such as electrocatalytic CO₂ and O₂ reduction, as well as metal-sulfur and redox-flow batteries. ¹⁻⁵ Critical to the performance of these electrodes is the interaction between the electric field, and the molecular species at the electrical double layer (EDL). Nevertheless, elucidating the potential/electric field experienced at the functionalized interface is challenging.

It has been shown, however, that the voltammetric response of electrodes functionalized with acidbase groups — either Brønsted species or redox-active molecules capable of proton-coupled electron transfer (PCET) — is sensitive to the energetics of proton transfer. These energetics are in turn a function not only of the pH of the electrolyte and pKa of the protonated species, but also the electrostatic potential. Consequently, by positioning such an electro-active group close to the surface of the electrode (i.e. within the EDL) and measuring its pH-dependent voltammetry, one can make inferences about the electrostatic potential/interfacial electric field profile at the electrode|electrolyte interface. This strategy has been applied to interpreting the capacitive behavior of gold electrodes coated with self-assembled monolayers (SAMs) of acid-terminal alkyl chains. ^{6,7} A number of recent studies have coupled pH-dependent SAM voltammetry with indirect measurements of electric field effects via spectroscopy. ⁸⁻¹⁰

An alternative system for studying electrostatic effects at aqueous electrolyte|electrode interfaces is that of the quinone-functionalized electrode. Quinones are PCET-active, and their intrinsic pKa and redox properties are widely tunable via substitution, making them a rich platform for exploring the relationship between EDL structure and proton-transfer energetics. Anthraquinones in particular have received considerable attention in this regard: several studies have explored variations in their kinetic properties and formal potential vs pH (i.e., Pourbaix) behavior upon noncovalent attachment to gold, 11-13 mercury 14,15, carbon 16-19 and indium tin oxide 5 electrodes. In all cases, PCET behavior is preserved upon quinone immobilization, but it is also typically observed that the electrode-bound quinone has an apparently stronger proton affinity (higher pKa) than its dissolved analogue, as evinced by a more negative average Pourbaix slope. This change in Pourbaix behavior has been attributed to a decrease in the local dielectric constant of water, from 78 in bulk solution to an effective value between 8 and 16 within the EDL, where the dense molecular film resides. This decrease in dielectric constant limits the ability of the electrolyte to effectively screen the electrode's surface charge, and therefore a strong electric field is felt at the quinone's redox center, which augments the chemical driving force for protonation of its reduced form. 14 Similar changes in Pourbaix behavior have been observed upon covalent conjugation of quinone to glassy carbon electrode via diazonium reduction.²⁰

Because the Pourbaix slope at a given pH is quantitatively related to the balance between protonated and deprotonated forms of the reduced quinone, it follows that changes in Pourbaix slope as a result of quinone immobilization also reflect variations in the electrostatic potential experienced by the quinone within the EDL. In principle, then, by varying the position of a quinone within the EDL and measuring the resultant Pourbaix behavior, one might be able to quantitatively elucidate the electrostatic potential profile at a given electrode|electrolyte interface.

In this work, we demonstrate that the method of conjugating a quinone to a carbon electrode can significantly alter its PCET behavior in a manner that is explicable based on the quinone's position within the EDL. In particular, we examine the PCET behavior of glassy carbon electrodes functionalized with 1-aminoanthraquinone-2-sulfonic acid (AAQS) via either amide coupling (Scheme 1a), facilitated by 1-ethyl-3-(3-dimethylaminopropyl) carbodiimide (EDC), (GC-EDC-AAQS), or radical-mediated diazonium reduction (Scheme 1b, GC-AAQS). GC-AAQS was found to have a more negative average Pourbaix slope than GC-EDC-AAQS, which exhibited similar Pourbaix behavior to its dissolved (molecular) analogue. The Pourbaix slope of GC-AAQS was also found to be more negative with decreasing electrolyte concentration. We attribute the more negative Pourbaix slope in GC-AAQS to the quinone being closer to the GC surface, and thus

exposed to stronger attractive electric field for protons. We determine how the measured Pourbaix slope is quantitatively related to the magnitude of the potential drop between the quinone and bulk solution. Lastly, using a simple multilayer dielectric (Gouy-Chapman-Stern) model of the EDL, we demonstrate how changes in the potential drop – and thus Pourbaix slope – as a result of variations in the electrolyte concentration, and distance between the ketone moiety and the GC surface, rationalize experimental trends. Our results highlight the potential for the use of PCET thermochemistry to map out the electric field/electrostatic potential profile at electrode|electrolyte interfaces of relevance to many emerging electrochemical technologies.

Methods

1-aminoanthraquinone-2-sulfonic acid, potassium permanganate (99%), 1-Ethyl-3-(3-dimethylaminopropyl) carbodiimide (97%), sulfuric acid (98%), acetic acid (99%), sodium monobasic phosphate (99%), sodium dibasic phosphate (99%), phosphoric acid (85%) and carbonate-bicarbonate buffer were purchased from Sigma Aldrich and used as received. Hydrochloric acid (37 wt. %) was purchased from Fisher and also used as received. Glassy carbon (GC) and edge plane pyrolytic graphite (EPPG) disks 5 mm in diameter were purchased from Pine Research and polished before oxidative treatment in potassium permanganate solution.

Amide- and Radical-Mediated Coupling of AAQS to Carbon

Prior to functionalization, each GC or EPPG electrode was polished successively on a series of polishing papers with roughness ranging between 5 μ m and 0.3 μ m for roughly 2 min each, and then rinsed thoroughly with deionized water (18.2 M Ω cm).

The procedure for the synthesis of GC covalently bound to AAQS via an amide bond (Scheme 1a) is adapted from Holm *et al.*²¹ The surface of GC was first chemically oxidized via immersion in 25 mM KMnO₄ (Sigma Aldrich) in a 1 M H₂SO₄ solution for 3 hours.²² This procedure is expected to increase the surface concentration of carboxylic acid groups, which will then serve as sites for amide coupling in the next step.²¹ The electrode was then washed with copious amounts of 0.1 M HCl to remove any MnO₂ precipitate, sonicated in deionized water for 2 minutes, and then dipped into a continuously stirred solution of 20 mM EDC in dichloromethane. After 30 minutes of stirring, 10 mM of AAQS was added. The reaction between the carboxylic acid groups and AAQS was allowed to proceed for 21 hours at room temperature, after which the electrode (now denoted GC-EDC-AAQS) was rinsed and sonicated in acetonitrile to remove weakly bound or otherwise physisorbed species.

The protocol for the fabrication of GC or EPPG electrodes covalently bound to AAQS via radical-mediated coupling (GC-AAQS and EPPG-AAQS) was adapted from several literature reports 18,20,23,24 in which an aromatic amine is first converted to a diazonium salt by reaction with a nitrite, and then reduced to form a radical. This method has been used for the covalent grafting of various substrates to a wide range of molecules ranging from quinones to glycol-proteins. Graphitic edge sites have been shown to be more active than the basal plane of carbon

for radical-mediated grafting. 32,33 Therefore, to promote the formation of the former in GC, each disk was first immersed in 25 mM KMnO₄ in 1 M H₂SO₄ for 3 hours and rinsed further to remove MnO₂ precipitate. Diazotization of AAQS was conducted as follows. 10 mM of AAQS was dissolved in a 0.5 M HCl solution and left to stir until completely dissolved. 10 mM of NaNO₂ was then added to the AAQS solution to form the diazonium salt. The electrode was then immersed into the solution and a reducing potential of -0.5 V vs. Ag/AgCl was applied for ~ 25 min. CV measurements were recorded in buffer solutions subjected to ~5 mins of degassing with nitrogen gas. We also subjected EPPG to this procedure, because it has a high concentration of active sites for diazonium reduction. 28

a)

KMnO₄

$$1M H_2SO_4$$

O

O

NH2

SO₃H

O

NAQS

Diazonium salt

O

NAD

O

NH2

SO₃H

O

O

NAD

O

Scheme 1. Reaction schemes showing (a) chemical oxidation of GC electrode to increase superficial population of -COOH groups, followed by dehydrative coupling with AAQS to form GC-EDC-AAQS in the presence of EDC and (b) diazonium salt formation from AAQS and radical-mediated diazonium reduction to form GC-AAQS

Each conjugated GC electrode was sonicated in water to eliminate physisorbed species. All cyclic voltammograms were recorded on a CHI 7013e potentiostat. For Pourbaix analysis, buffer solutions with varied ionic strengths were prepared (see SI for details on buffer composition).

X-ray Photoelectron Spectroscopy (XPS) Measurements

XPS measurements were carried out on a Kratos Axis Ultra DLD spectrometer with a monochromatic Al K_{α} excitation source. Samples were placed on an indium tin oxide (ITO) sample

holder covered with copper tape before transfer to the XPS vacuum chamber. Before data collection, the chamber was evacuated to $\sim 2 \times 10^{-8}$ Torr. XPS data were collected at an incidence angle of 54.7° relative to the analyzer axis. Survey scans (0 – 1200 eV), were collected at pass energy of 160 eV with a 1 eV step size and 5 spectral sweeps. High-resolution core scans for carbon, oxygen, nitrogen and sulfur were then recorded. Peak fittings were done in CasaXPS with a Shirley baseline and equal constraints for the full width at half max for each fitting until all peaks were fully resolved. All species were charge corrected with reference to main carbon 1s peak at 248.8 eV.

Results & Discussion

<u>Derivatization of Carbon Electrodes</u>

GC electrodes were covalently functionalized with AAQS via two distinct methods (Scheme 1) that have been previously described in the literature: (1) diazotization and coupling via radical-mediated diazonium reduction, ^{28,31,34-36} and (2) dehydrative coupling to carboxylic acid groups on chemically oxidized GC in the presence of 1-ethyl-3-(3-dimethylaminopropyl) carbodiimide (EDC). ^{21,22} The resulting electrodes are denoted GC-AAQS and GC-EDC-AAQS, respectively. These different derivatization methods were expected to result in different AAQS structures at the electrode-electrolyte interface, and thus different potential drops between the redox-active quinone moieties and the GC surface, which would result in distinct PCET (Pourbaix) thermochemistry. AAQS is an ideal molecular motif for these studies because its sulfonic acid functional group confers aqueous solubility to the molecule; this makes Pourbaix analysis of the dissolved form possible and the primary amine group permits the attachment of AAQS to carbon.

In the procedure for fabricating GC-AAQS, the oxidative treatment promotes the formation of sp³-type and oxidized species on carbon after this treatment. This is supported by X-ray photoelectron spectroscopy (XPS) measurements (Figure S1). As shown in Scheme 1b, the addition of NaNO₂ to AAQS resulted in the conversion of the amine to a diazonium salt. A slight color change from a deep to milky orange was observed after the addition of NaNO₂ (Figure S2), and measurement of the solution's optical absorbance via UV-vis spectroscopy showed the disappearance of the broad absorbance peak of AAQS at 480 nm, consistent with the formation of an anthraquinone-based diazonium salt.³⁷ Electrochemical reduction of the diazonium group was intended to neutralize the diazonium group, resulting in the release of N₂ and formation of a radical that could bind strongly and irreversibly to the carbon surface (see Scheme 1b). However, no reduction peaks were observed at potentials higher than the redox potential of the quinone (Figure S3), which is where irreversible diazonium reduction tends to occur.^{20,23} We therefore believe a spontaneous chemical reduction is likely to be responsible for the formation of GC-AAQS, which is known to result in a weaker covalent bond between GC and AAQS relative to what is expected for binding initiated by electrochemical reduction.^{18,19,27,34}

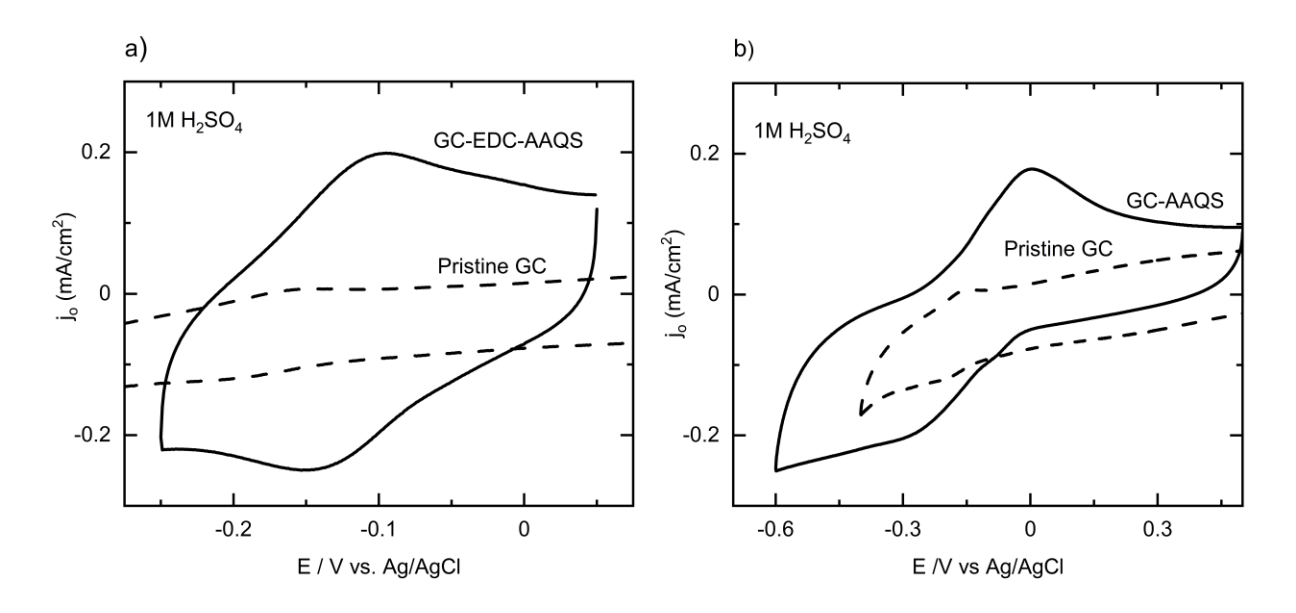


Figure 1. CVs for pristine (unmodified) GC (dotted lines), a) GC-EDC-AAQS and b) GC-AAQS in 1 M H₂SO₄. No redox activity observed on unconjugated GC electrode

Cyclic voltammogram (CV) measurements of GC-EDC-AAQS and GC-AAQS in 1 M H₂SO₄ (Figure 1) revealed redox peaks (as calculated from the midpoint between the voltages of peak anodic and cathodic current) centered on -0.12 V and -0.14 V vs Ag/AgCl respectively. These peaks are not present in an unmodified GC electrode; we therefore attribute them to 2H⁺, 2e⁻ PCET involving the quinone. CVs on GC-AAQS and GC-EDC-AAQS taken at different scan rates are consistent with the quinone moiety being attached to the GC surface rather than dissolved in solution. Specifically, in both cases, peak currents were linearly proportional to the scan rate in 1M H₂SO₄ (Figure S4); this linear relationship is retained in 1 M KOH as well (Figure S5). For dissolved AAOS, peak current was proportional to the square root of scan rate under acidic and alkaline conditions (Figure S6), as is expected for a mass-transport-limited redox reaction. We estimated quinone surface coverage from the anodic Faradaic charge at each scan rate for CVs taken in 1 M H₂SO₄ and 1 M KOH (Figure S7). The area under the redox peak was calculated using the "peak and baseline" function in Origin. With this option, one can draw a baseline that matches the slope of the capacitive current on either side of a given redox peak. This artificial baseline was then subtracted from the raw CV and the resulting area under the peak is calculated as the Faradaic charge. At 100 mV/s in 1 M H₂SO₄, this procedure yielded nominal quinone surface coverages (Γ) of 1.68 ×10⁻⁹ and 6.48 ×10⁻¹⁰ mol/cm² for $\Gamma_{GC\text{-}AAOS}$ and $\Gamma_{GC\text{-}EDC\text{-}}$ AAOS, respectively. These values are consistent with each electrode being covered by a statistical monolayer of AAQS; estimates for the surface coverage of close-packed phenyl groups on a planar carbon surface range between 6.5 ×10⁻¹⁰ and 1.4 ×10⁻⁹ mol/cm². ^{31,38} Nevertheless, our measured surface coverage values are likely overestimates of the true coverage, as the GC surface is not atomically flat, meaning its actual surface area is greater than its geometric area. It is also worth noting that our CV and spectroscopic data cannot entirely rule out the formation of partial multilavers on GC-AAOS that are caused by some fraction of quinone radicals attacking deposited AAQS, rather than glassy carbon.³⁹

We also conjugated AAQS onto an edge plane pyrolytic graphite electrode (EPPG-AAQS) via diazonium reduction, using the same procedure as for GC. EPPG was chosen because graphitic edge sites are known to be especially active for diazonium reduction.²⁸

Characterization of Surface Chemistry of Modified GC Electrodes

X-ray photoelectron spectroscopy (XPS) was used to characterize the surface chemistry of AAQS and the modified GC electrodes. Survey scans for AAQS powder, chemically oxidized GC, GC-AAQS and GC-EDC-AAQS are shown in Figure S8. Each spectrum exhibited peaks from carbon and oxygen; nitrogen and sulfur peaks were also present in AAQS, as expected. Manganese was found in oxidized GC and GC-EDC-AAQS electrodes, which we attribute to the incomplete removal of solid MnO₂.

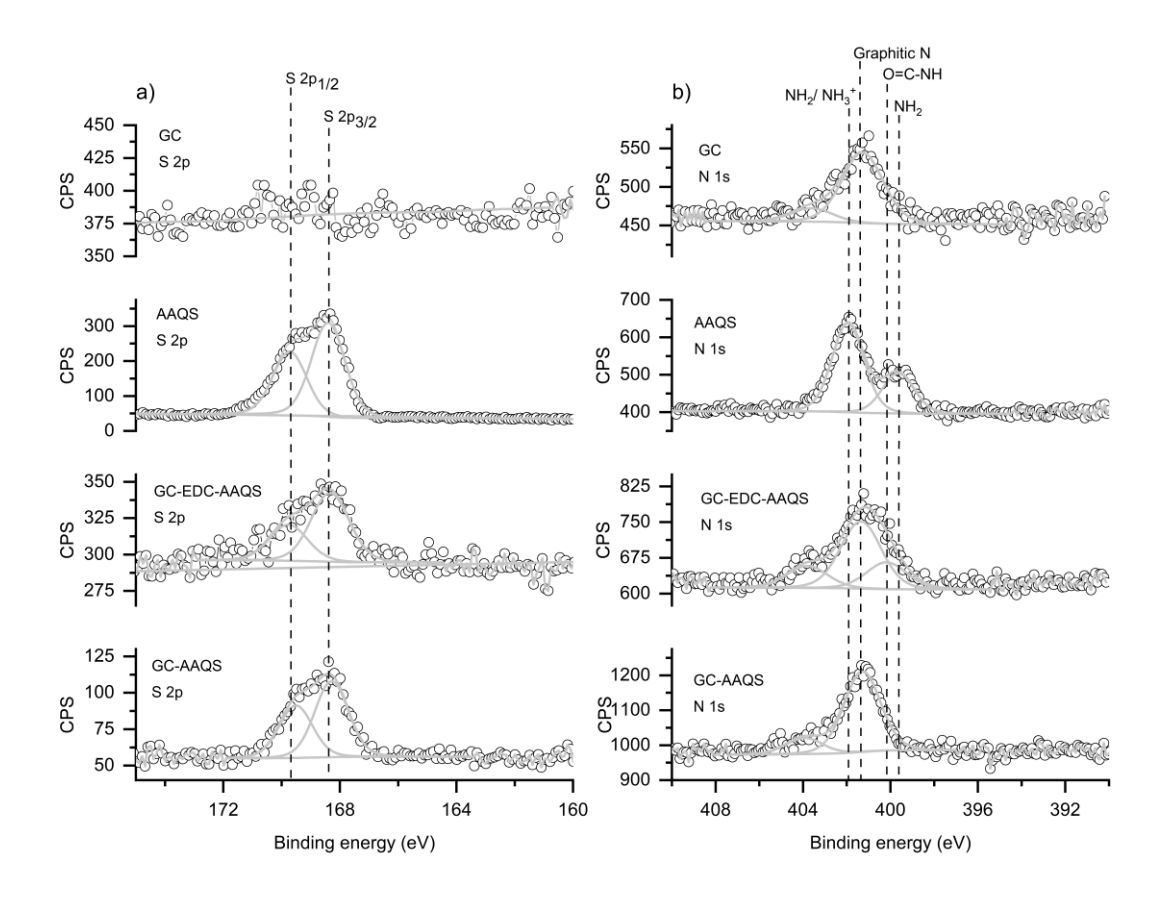


Figure 2. (a) S 2p and (b) N 1 s spectra of AAQS, GC-AAQs and GC-EDC-AAQS.

Figure 2a reports the high-resolution spectrum of the S 2p region where, as expected, no peaks were observed for the unmodified GC electrode. The sulfonate group in AAQS is present as a single doublet from S 2p^{3/2} and S 2p^{1/2} at 167.8 eV and 169.0 eV, respectively.^{40,41} S 2p peaks at the same binding energies appear in GC-AAQS and GC-EDC-AAQS, which means that the chemical environment around the sulfonate functional group is preserved upon modification of GC.

Curve fits to high-resolution spectra of the N 1s region (Figure 2b) are consistent with the structures for GC-EDC-AAQS and GC-AAQS shown in Scheme 1. The binding energy for the nitrogen from the amine group on AAQS is 399.6 eV. 17,42,43 This peak is absent in GC-AAQS and GC-EDC-AAQS, consistent with loss of the amine via its conversion to diazonium and release as N₂. In GC-EDC-AAQS, a new peak appeared at 400.1 eV, in agreement with nitrogen in an amide bond. 43-46 In GC, GC-EDC-AAQS and GC-AAQS, we observed a significant component of the N 1s spectrum at 401.1 eV, which we attribute to graphitic nitrogen. 43 In AAQS powder, we also observed a peak at a high binding energy (BE) of 401.9 eV, which may originate from some fraction of the amine groups in AAQS being protonated (i.e. -NH₃+). This assignment is plausible because AAQS is synthesized using sulfuric acid. 47

Further corroboration of the above assignments is provided by C 1s and O 1s spectra. Following oxidative treatment of GC, a peak evolved at 286.5 eV in the C 1s spectra, which is consistent with the formation of carbonyl (C=O)-type species (Figure S1). We also observed a peak at ~285.3 eV in AAQS alone (Figure S9), which is the BE expected for a C-N bond. The other C-N bond appears only in GC-EDC-AAQS as an amide, which has a distinct peak at ~286.9 eV. In the O 1s spectrum for GC-EDC-AAQS, a peak is present at ~535.4 eV which is also attributable to the formation of the amide bond (Figure S10). The absence of the C-N bond in GC-AAQS agrees with conversion of the amine group in AAQS to its corresponding diazonium salt and subsequent elimination as N_2 . (Figure S9).

Electrochemical Behavior and Pourbaix Analysis of Dissolved vs Carbon-Conjugated AAQS.

CVs for dissolved AAQS, GC-EDC-AAQS, GC-AAQS, and EPPG-AAQS between pH 3 and 13 are reported in Figure 3a-d. CVs for dissolved AAQS on EPPG can be found in Figure S11. Surface coverage of 3.43 ×10⁻¹⁰ mol/cm² in 0.1 M KOH buffer at 100 mV/s) was obtained for EPPG-AAQS. Acetate, phosphate and bicarbonate buffers with a fixed total concentration of 0.1 M were used. Between pH 2 and 7, the average Pourbaix slopes for dissolved AAQS on GC, GC-EDC-AAQS and GC-AAQS and EPPG-AAQS were -54.5 mV/pH, -52.2 mV/pH, -49.7 mV/pH and -56.8 mV/pH respectively (Figure 3e), which are roughly consistent with one proton per electron transferred and in agreement with prior Pourbaix measurements of sulfonated anthraquinones. ^{50,51} Between pH 7 and 10, the Pourbaix slopes of GC-EDC-AAQS and dissolved AAQS increased above those of GC-AAQS and EPPG-AAQS. Above pH 10, the divergence was more pronounced

(Figure 3e). The Pourbaix slopes calculated from CVs for dissolved AAQS (Figure 3a) and GC-EDC-AAQS (Figure 3b) were -8.7 mV/pH and -6.6 mV/pH, respectively, consistent with the reduction of AAQS to a largely deprotonated form, i.e. with a second pKa for the protonated reduced form around 10. Similar Pourbaix behavior was observed for anthraquinone-2-sulfonic acid (Figures S12 – 13), which is the molecular analogue to GC-AAQS. For GC-AAQS (Figure 3c) and EPPG-AAQS (Figure 3d), we observed Pourbaix slopes between pH 10 and 13 of –51.7 mV/pH and -36.1 mV/pH, which are consistent with H⁺:e⁻ ratios closer to 1:1 and 1:2 H⁺:e⁻, respectively.

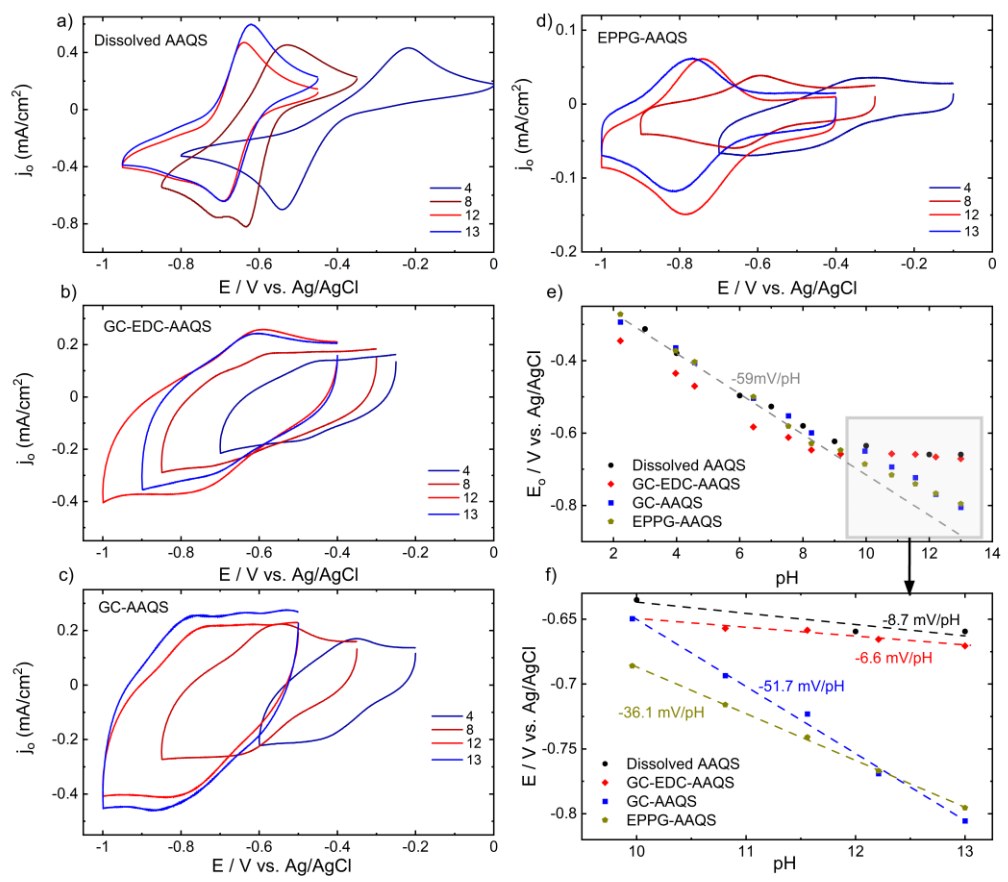


Figure 3. CVs for (a) dissolved AAQS (b) GC-EDC-AAQS (c) GC-AAQS (d) EPPG-AAQS in 0.1 M buffers. (e) Pourbaix diagram for dissolved AAQS, and electrode-conjugated AAQS between pH 2 and 13. A zoomed-in view of the pH 10-13 region is shown in (f).

These Pourbaix slope trends indicate that the method of covalent attachment of AAQS to GC can have a profound effect on PCET behavior. We hypothesize that these trends in PCET can be explained on the basis of varying fractions of the metal-solution potential drop felt by AAQS; these variations might originate from different positions of the redox-active quinone moiety in conjugated or dissolved AAQS within the EDL. Specifically, the closer the quinone moiety is to the GC surface, the more closely the shift in the potential it experiences tracks potential shifts imposed at the GC surface, which in turn influences PCET thermochemistry. Because dehydrative

EDC coupling generates an amide bond between GC and AAQS (Scheme 1a) – leaving the quinone moiety farther from the GC surface than in GC-AAQS – GC-EDC-AAQS exhibits similar electrochemistry to its molecular AAQS analogue.

We exclude the possibility that the trends observed here stem primarily from physisorption of AAQS to GC as reported in literature. ^{24,33,52} We soaked a highly absorbent graphite felt electrode in an acidic AAQS solution for 21 hours, and found that its Pourbaix behavior (Figure S14) was almost identical to that of dissolved AAQS. Changes in the chemical environment of nitrogen, as evidenced by binding energy shifts in the N 1s spectra discussed above, are likewise inconsistent with physisorption playing a controlling factor in the electrochemical behavior of AAQS-functionalized electrodes.

Modeling the Effect of AAQS Conjugation to GC on PCET Thermochemistry

We propose that the differing Pourbaix slopes observed for dissolved AAQS, GC-EDC-AAQS and GC-AAQS beyond pH 10 can be explained by different electrostatic potentials experienced by the reduced quinone within the EDL, and thus different driving forces for PCET.⁵³ In the absence of an electric field, PCET will be entirely determined by the difference between the intrinsic pKa of the reduced quinone (hence denoted the "zero-field" pKa, or pKa_{0-field}) and the electrolyte pH: if pH < pKa_{0-field} of the reduced form, PCET will occur and the reduced quinone will be fully protonated, whereas if pH > pKa_{0-field}, the reduced quinone remains deprotonated.⁵⁴ In the presence of an electric field, however, PCET may occur even if pH > pKa_{0-field}, as the electric field within the EDL may alter the driving force for protonation of the reduced form.⁵⁵ Consequently, because the Pourbaix slope at any given pH reflects the degree of protonation of the reduced form, it also reflects the electrostatic potential profile at the modified GC|electrolyte interface if the slope is non-zero and pH > pKa_{0-field}.

To quantify the relationship between the Pourbaix slope and the potential distribution, we first consider that upon electrochemical reduction, the quinone may either remain fully protonated, or dissociated into a singly or doubly deprotonated form; we denote these as RH₂, RH⁻ and R², respectively. The full reaction may be written as follows:

$$0 + 2e^{-} + 2H^{+} \leftrightarrow RH_{2} \leftrightarrow RH^{-} + H^{+} \leftrightarrow R^{2-} + 2H^{+}$$
 (1)

At equilibrium the sum of electrochemical potentials for reactants and products for each of the three chemical or electrochemical reactions should be equal. The electrochemical potential for each species $(\bar{\mu}_i)$ can be expressed as the sum of its chemical and electrostatic components:

$$\bar{\mu}_i = \mu_i^0 + RT \ln a_i + zF \Phi_i$$
 (2)

where R is the universal gas constant (8.314 J mol⁻¹K⁻¹), T is temperature (assumed to be 298 K), a_i is activity of chemical species i, z is charge, F is Faraday's Constant (96485 C mol⁻¹) and Φ is electrostatic potential. To avoid using the concept of an absolute potential in the electrochemical

reaction above, we follow Smith and White⁵³ in representing it in terms of a complete cell with a half-cell reaction involving an ideally nonpolarizable Ag/AgCl reference electrode (AgCl + $e^- \leftrightarrow$ Ag + Cl⁻). The electrochemical reaction may now be rewritten as:

$$O + 2e_{M}^{-} + 2Ag + 2Cl^{-} + 2H^{+} \leftrightarrow RH_{2} + 2AgCl + 2e_{Ag}^{-}$$
 (3)

and electrochemical equilibrium requires that

$$\bar{\mu}_{O} + 2\bar{\mu}_{e-,M} + 2\bar{\mu}_{H+} + 2\bar{\mu}_{Ag} + 2\bar{\mu}_{Cl-} = \bar{\mu}_{RH2} + 2\bar{\mu}_{AgCl} + 2\bar{\mu}_{e-,Ag}$$
 (4)

where electrons in the working electrode and reference electrodes bear the subscripts "M" and "Ag", respectively. By taking account of the fact that the standard free energy of the above reaction $\Delta G^{o} = -nFE^{o}$, $E = \Phi_{M} - \Phi_{Ag}$, and assuming the activity of Cl⁻ ions is 1, we obtain the Nernst Equation:

$$E = E^{o} + \frac{RT}{2F} \ln \frac{a_{o} a_{H+}}{a_{RH2}}$$
 (5)

where E and E^o are now, by definition, referenced to Ag/AgCl. The proton dissociation equilibria require that

$$\bar{\mu}_{RH_2}^{PET} = \bar{\mu}_{H^+}^{PET} + \bar{\mu}_{RH^-}^{PET} = \bar{\mu}_{R^{2-}}^{PET} + 2\bar{\mu}_{H^+}^{PET}$$
 (6)

where "PET" denotes the "plane of electron transfer." For RH₂, RH⁻ and R²⁻, z = 0, -1 and -2 respectively. We ignore the negative charge on the sulfonate group of AAQS, because the sulfonic acid group of benzenesulfonic acid has a pKa of – 2.8,⁵⁶ and AAQS will thus remain deprotonated at all pH values relevant to this study. By substituting the appropriate expressions for electrochemical potentials into Equation (6), and assuming the electrochemical potential of the proton at the PET is equal to that in the bulk, the first equality in Equation (6) becomes:

$$\mu_{RH_2}^0 - \mu_{RH^-}^0 - \mu_{H^+}^0 + RT \ln \frac{a_{RH_2}}{a_{RH^-} a_{H^+}} = F(\Phi_S - \Phi_{PET})$$
 (7)

Replacing activities with concentrations, the acid dissociation constants for the first and second deprotonation events (K_{a1} and K_{a2}) in the absence of an electric field are:

$$K_{a1} = \frac{[H^+][RH^-]}{[RH_2]}$$
 and $K_{a2} = \frac{[H^+][R^{2-}]}{[RH^-]}$ (8)

Using the relationship between each dissociation constant and reaction Gibbs free energy, we relate the free energy of RH_2 deprotonation to K_{a1} :

$$-\Delta G = \mu_{RH_2}^0 - \mu_{RH^-}^0 \mu_{H^+}^0 = RT \ln (K_{a1})$$
 (9)

Substituting this expression into Equation (7) yields

$$-2.3RT(pKa_{(1,0-field)}) + ln \frac{a_{RH_2}}{a_{RH^-} a_{H^+}} = -\frac{F}{RT} (\Phi_{PET} - \Phi_S)$$
 (10)

where pKa_(1,0-field) = $-\log K_{a1}$. The potential drop between the PET and bulk solution will be some fraction, f, of the total drop from the electrode to solution. Therefore, $(\Phi_{PET} - \Phi_S) = f(\Phi_M - \Phi_S)$. $\Phi_M - \Phi_S$ is, by definition, equal to $E - E_{PZC}$, where E_{PZC} is the potential of zero charge, and can take any value between 0 and 1. For the more acidic hydroquinone proton in RH₂, Equation (10) becomes:

$$-2.3RT(pKa_{(1,0-field)}) + ln \frac{a_{RH_2}}{a_{RH^-} a_{H^+}} = -\frac{F}{RT} f_1(E - E_{PZC})$$
 (11)

where f_1 is the fraction of the full potential drop felt at the site of the more acidic proton. Similar analysis for the less acidic proton in RH₂ yields:

$$-2.3RT(pKa_{(2,0-field)}) + ln \frac{a_{RH^-}}{a_{R^{2-}}a_{H^+}} = -\frac{F}{RT}f_2(E - E_{PZC})$$
(12)

By assuming activities of all surface quinone species are equal to surface concentrations, and denoting each surface concentration as a fraction of the total quinone concentration, it follows from mass conservation that:

$$a_0 + a_{RH2} + a_{RH-} + a_{R2-} = 1 \tag{13}$$

Equations (5), (11), (12) and (13) comprise a system of equations that govern the distribution of O, RH₂, RH⁻ and R²⁻ and can be solved for any choice of pH, pKa_{0-field} values, E, E⁰, E_{PZC}, f_1 and f_2 .

We solved the system of equations analytically to obtain the concentration of the four species mentioned above for any possible potential and pH value. The solution of Equations (5), (11), (12) and (13) are:

$$a_{\rm O} = \frac{p^2}{p^2 + a_{\rm H^+}^2 + K_{a1} a_{\rm H} p^{f_1} q^{f_1} + K_{a1} K_{a2} p^{f_1 + f_2} q^{f_1 + f_2}}$$
(14)

$$a_{\text{RH}_2} = \frac{a_{\text{H}^+}^2}{p^2 + a_{\text{H}^+}^2 + K_{a1} a_{\text{H}} p^{f_1} q^{f_1} + K_{a1} K_{a2} p^{f_1 + f_2} q^{f_1 + f_2}}$$
(15)

$$a_{\text{RH}^{-}} = \frac{K_{a1} \, a_{\text{H}} \, p^{f_1} q^{f_1}}{p^2 + a_{\text{H}^{+}}^2 + K_{a1} \, a_{\text{H}} \, p^{f_1} q^{f_1} + K_{a1} K_{a2} p^{f_1 + f_2} q^{f_1 + f_2}}$$
(16)

$$a_{R^{2-}} = \frac{K_{a1}K_{a2}p^{f_1+f_2}q^{f_1+f_2}}{p^2 + a_{H^+}^2 + K_{a1} a_H p^{f_1}q^{f_1} + K_{a1}K_{a2}p^{f_1+f_2}q^{f_1+f_2}}$$
(17)

where $p = \exp\left[\frac{2F}{RT}(E - E_0)\right]$ and $q = \exp\left[\frac{2F}{RT}(E_0 - E_{PZC})\right]$. The Pourbaix slope for any set of electrochemical parameters is the plot of E vs pH for which $a_0 = a_{RH2} + a_{RH-} + a_{R2-}$, i.e. where the concentration of reduced and oxidized species is equal. Therefore, to obtain a given Pourbaix plot, we looked up the value of E for which $a_0 = 0.5$ within a given pH range. Figure 4a compares experimental and simulated Pourbaix slopes for dissolved AAQS. We found good agreement for pKa_{1,0-field} and pKa_{2,0-field} values of 7 and 11 respectively. E_{PZC} was fixed at 0.086 V vs Ag/AgCl based on literature precedent for glassy carbon.⁵⁷ f_1 and f_2 were set to zero given that dissolved AAQS, being negatively charged, is likely close to the edge of or beyond the EDL, and will thus experience a negligible fraction of the electrode-solution potential drop. These results are consistent with PCET being strongly determined by the intrinsic chemical affinity of R²⁻ for protons, rather than the interfacial electric field – this proposition is consistent with the Pourbaix slope approaching zero as the pH exceeds pKa_{0-field}.

In contrast, the more negative Pourbaix slopes for pH > pKa_{0-field} in electrode-conjugated AAQS (Figure 3f), are explained by larger values of f_1 and f_2 , presumably as a result of the closer proximity of the redox head groups to the electrode surface. In Figure 4b, we demonstrate that the experimental Pourbaix behavior for GC-AAQS and EPPG-AAQS are reasonably well reproduced by a simulation in which f_1 and f_2 are 0.15 and 0.7, respectively.

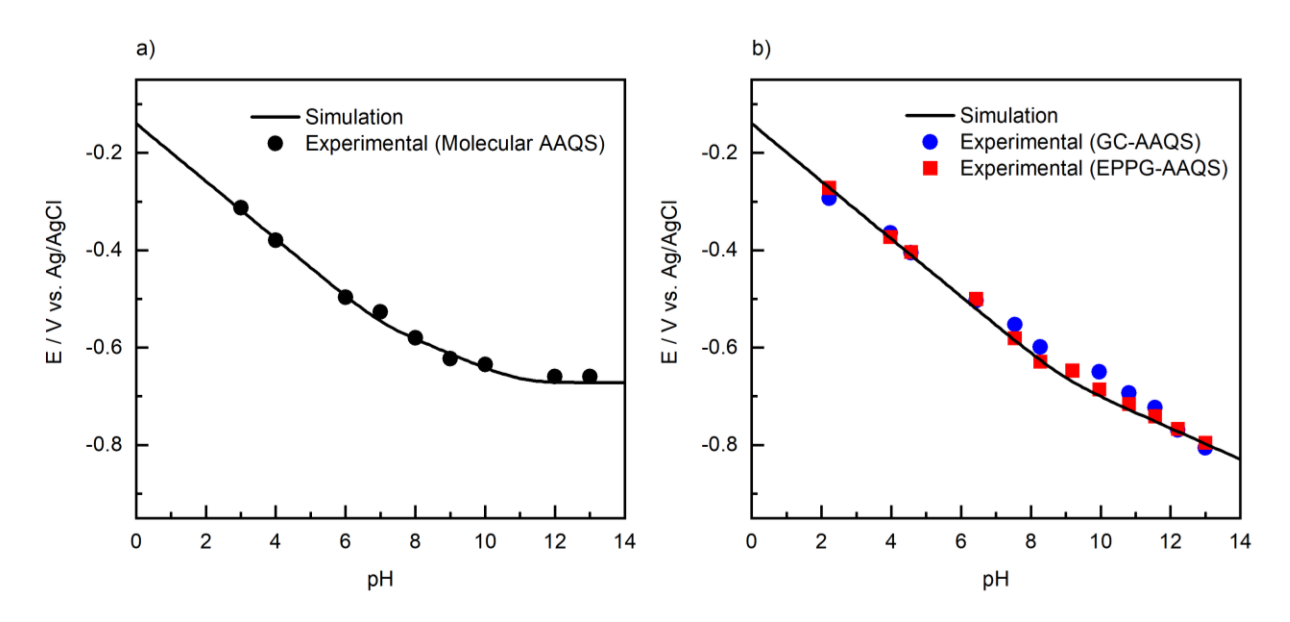


Figure 4. a) Experimental and simulated Pourbaix for dissolved AAQS. Pourbaix slopes for pH 0-7: -58.6 mV/pH (simulated); -54.5 mV/pH (experimental). b) Simulated Pourbaix slope was fitted to experimental data for f_1 and f_2 values at 0.15 and 0.7. Pourbaix slopes past pH 10: -32.2 mV/pH (simulated), -36.1 mV/pH (EPPG-AAQS), -51.7 mV/pH (GC-AAQS).

We have assumed in this analysis that pKa_{0-field} of the reduced, protonated quinone – i.e., its intrinsic proton affinity, in the absence of field effects – is fixed regardless of whether or not it is tethered to an electrode. It is possible, however, that pKa_{0-field} of the quinone might change upon electrode fixation due to a change in molecular orientation, electron withdrawal or donation by covalent bonding to electrode species, loss of functional groups that are vicinal to the diketone group, or other effects. Separating the influence of these factors from the influence of the EDL on PCET is beyond the scope of this work. Nevertheless, one could approach this question by coupling voltammetry to another technique that is directly sensitive to the polarization state of the quinone, such as *operando* x-ray absorption or photoelectron spectroscopy (*vide infra*).

Effect of Electrolyte Concentration on PCET

At a given pH, decreasing the buffer concentration is expected to increase the thickness of the EDL (Figure S15). According to the reasoning presented above, this change will decrease $\Phi_{PET} - \Phi_{S}$ and thus increase f, which will decrease the average Pourbaix slope for a given pH range. We evaluated this possibility by measuring in quadruplicate the Pourbaix behavior of GC-AAQS for buffer concentrations of 5, 10, 50, 100 mM and 1 M, and for pH values above 10 (CVs from a representative set of measurements are shown in Figure S16). There is considerable variation in the absolute value of the Pourbaix slope between replicates. Nevertheless, as expected, the average Pourbaix slope (Figure 5a) decreases with decreasing buffer concentration from -39.1 mV/pH at 1 M to -52.4 mV/pH at 5 mM. Figure 5b presents simulated $\Phi_{PET} - \Phi_{S}$ vs buffer concentration using the Gouy-Chapman-Stern EDL model. We assumed the distance between the redox center and electrode surface, d, was 0.5 nm, and dielectric constants of 7 and 78 within and outside the Stern layer, respectively. As buffer concentration decreases, $\Phi_{PET} - \Phi_{S}$ decreases, which should result in an increase in f (i.e. an increase in $(\Phi_{PET} - \Phi_S)/(\Phi_{app} - \Phi_S)$, see Figure S17a). In addition, we observed that the magnitude of $\Phi_{PET} - \Phi_{S}$ decreases as d increases (Figure S17b), which would result in a lower value of f. These trends correspond qualitatively to our experimental observations if one allows that d is higher for GC-EDC-AAQS and molecular AAQS than GC-AAQS and EEPG-AAQS.

Our work suggests that it is possible to elucidate the potential profile at functionalized electrode|electrolyte interfaces by measuring the Pourbaix behavior of PCET-active redox moieties that are conjugated within a small distance from the electrode surface. Insights from such measurements may be applied in various aspects of electrochemical science and technology, from assessing modern theories of EDL structure to promoting electrocatalysis via appropriately tuned interfacial electric fields, to designing redox electrodes for pH-swing-driven CO₂ capture⁵⁸⁻⁶¹ and other pH-sensitive chemical separations.⁶² In our future work, we will more directly probe the relationships among the quinone's structure and orientation with respect to the electrode surface, the applied potential, and the interfacial electric field/electrostatic potential experienced at the PET. This can be done by combining a variety of high-resolution scattering and spectroscopic techniques. Previous work has shown, for instance, that the magnitude of the BE shift for an element at an electrode|electrolyte interface is sensitive to the change in the electric field it experiences upon polarization of the electrode.⁶³⁻⁶⁵ Because sulfur is present in AAQS but not the GC (Figure 2a) or electrolyte, measuring its BE shift upon polarization may yield direct insight

into $\Phi_{\text{PET}} - \Phi_{\text{S}}$ and therefore f. To investigate the influence of PET-electrode distance on Pourbaix behavior and the interfacial potential, one may vary the nominal quinone-electrode distance by varying the number of benzene units between the ketone moiety and electrode, from zero for a benzoquinone, to one for an anthraquinone and two for tetracenedione (Figure S18). Understanding how Pourbaix behavior varies among these various species, and as a function of buffer concentration and surface coverage will yield a wealth of insight into EDL structure and dynamics.

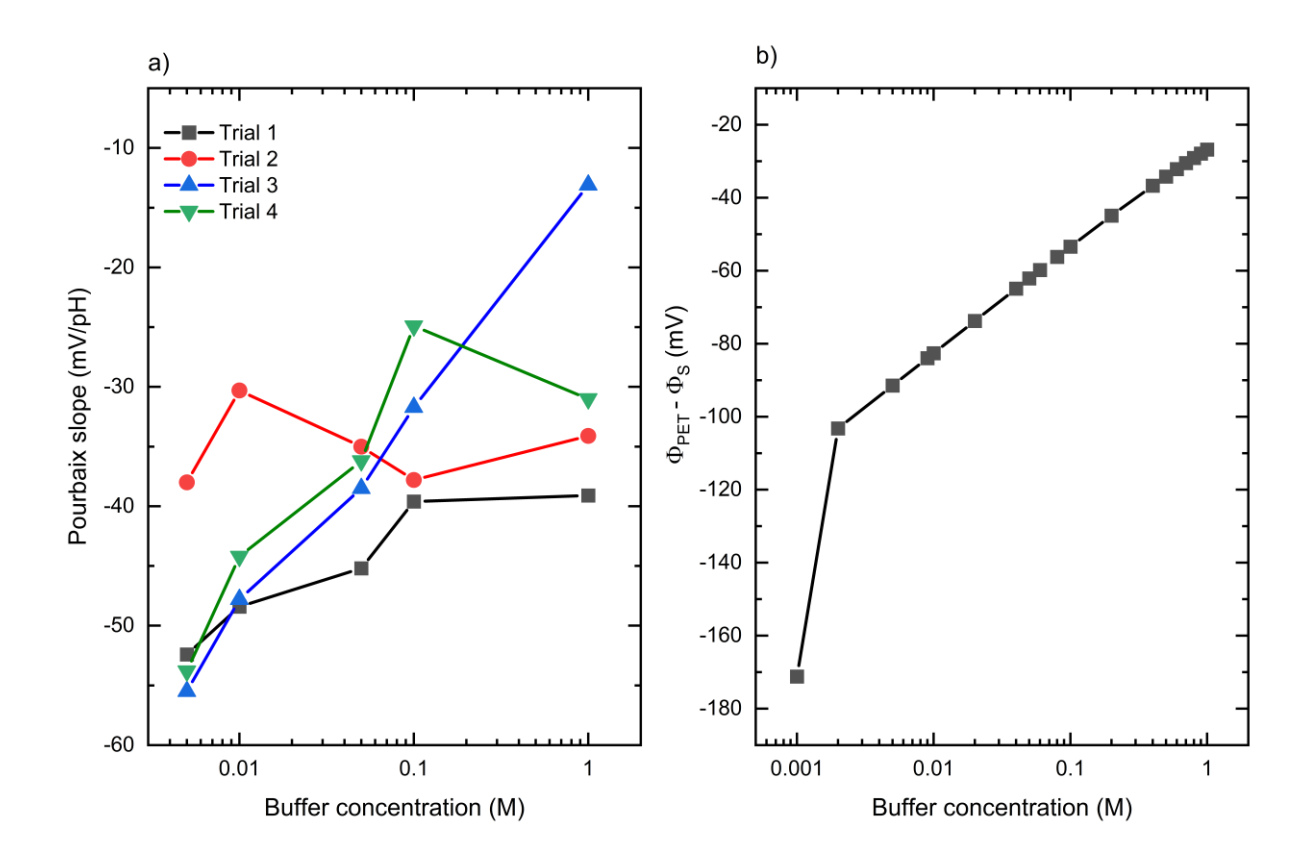


Figure 5. (a) Relationship between buffer concentration and experimental Pourbaix slope. Increasing buffer concentration results in a smaller Debye length and less negative Pourbaix slope. (b) Simulated electrostatic potential drop between the quinone's plane of electron transfer (PET) and solution vs buffer concentration. The plot was obtained via Equation S7, with $\varepsilon_1 = 7$, $\varepsilon_2 = 78$, d = 0.5 nm, and $\Phi_M = -0.5$ V.

Conclusions

We investigated the Pourbaix behavior of carbon electrodes that were functionalized with 1-aminoanthraquinone-2-sulfonic acid (AAQS) via two conjugation techniques: amide coupling and radical-mediated diazonium reduction. The two conjugation routes gave rise to electrodes with distinct redox potential vs pH (i.e., Pourbaix) slopes, suggestive of distinct proton-coupled electron transfer (PCET) energetics. We derived from the measured Pourbaix slope the potential drop

experienced by the ketone moiety in each quinone. Additionally, using a simple Gouy-Chapman-Stern model of the EDL, we have shown how varying PCET energetics as a function of AAQS conjugation mode and electrolyte concentration can be explained in large part by differing distances between the ketone moiety in each quinone and the electrode, and thus differing driving forces for interfacial electric field-driven protonation of the reduced quinone. Our results highlight the potential for the use of PCET thermochemistry to map out the electric field/electrostatic potential profile at electrode|electrolyte interfaces of relevance to many emerging electrochemical technologies. They could also inform the design of redox-active, chemically modified electrodes that can be integrated into flow cells designed to accomplish pH-sensitive chemical separations such as CO₂ capture, as well as nitrogen, phosphate or struvite recovery from wastewater.

Author Information

Corresponding author

David G. Kwabi - Department of Mechanical Engineering, University of Michigan, Ann Arbor, Michigan, 48109, United States. **Email:** dkwabi@umich.edu

<u>Author</u>

Fiki V. Owhoso - Department of Chemical Engineering, University of Michigan, Ann Arbor, Michigan, 48109, United States. **Email:** fikio@umich.edu

Sanat V. Modak - Department of Mechanical Engineering, University of Michigan, Ann Arbor, Michigan, 48109, United States. Email: sanat@umich.edu

Partha Saha - Department of Mechanical Engineering, University of Michigan, Ann Arbor, Michigan, 48109, United States. **Email:** parthasa@umich.edu

Supporting Information

Cyclic voltammograms of conjugated and molecular analogues of AAQS, XPS of conjugated electrodes, model of conjugated electrode are provided in the supporting information.

Acknowledgements

This work was funded by the National Science Foundation under Award Number 2045032. The authors acknowledge the financial support of the University of Michigan College of Engineering and NSF grant #DMR-0420785, and technical support from the Michigan Center for Materials Characterization.

References

- Ren, G.; Lu, X.; Li, Y.; Zhu, Y.; Dai, L.; Jiang, L. Porous Core–Shell Fe3C Embedded Ndoped Carbon Nanofibers as an Effective Electrocatalysts for Oxygen Reduction Reaction. *ACS App. Mat. & Inter.* **2016**, *8*, 4118-4125.
- Zhang, S.; Fan, Q.; Xia, R.; Meyer, T. J. CO2 Reduction: From Homogeneous to Heterogeneous Electrocatalysis. *Acc. of Chem. Res.* **2020**, *53*, 255-264.
- Zhao, C.-X.; Li, X.-Y.; Zhao, M.; Chen, Z.-X.; Song, Y.-W.; Chen, W.-J.; Liu, J.-N.; Wang, B.; Zhang, X.-Q.; Chen, C.-M.; et al. Semi-Immobilized Molecular Electrocatalysts for High-Performance Lithium–Sulfur Batteries. *J. Am. Chem. Soc.* **2021**, *143*, 19865-19872.
- Murray, R. W.; Goodenough, J. B.; Albery, W. J. Chemically modified electrodes for electrocatalysis. *Phil. Trans. Roy. Soc. Lond. Series A, Math. and Phy. Sc* **1981**, *302*, 253-265.
- Hanna, C. M.; Luu, A.; Yang, J. Y. Proton-Coupled Electron Transfer at Anthraquinone Modified Indium Tin Oxide Electrodes. *ACS App. En. Mat.* **2019**, *2*, 59-65.
- 6 Smiljanić, M.; Adam, C.; Doneux, T. Electric field induced proton transfer at α,ω-mercaptoalkanecarboxylic acids self-assembled monolayers of different chain length. *J. Electroanal. Chem.* **2018**, *815*, 238-245.
- White, H. S.; Peterson, J. D.; Cui, Q.; Stevenson, K. J. Voltammetric Measurement of Interfacial Acid/Base Reactions. *J. Phys. Chem. B* **1998**, *102*, 2930-2934.
- 8 Ge, A.; Kastlunger, G.; Meng, J.; Lindgren, P.; Song, J.; Liu, Q.; Zaslavsky, A.; Lian, T.; Peterson, A. A. On the Coupling of Electron Transfer to Proton Transfer at Electrified Interfaces. *J. Am. Chem. Soc.* **2020**, *142*, 11829–11834.
- Delley, M. F.; Nichols, E. M.; Mayer, J. M. Interfacial Acid–Base Equilibria and Electric Fields Concurrently Probed by In Situ Surface-Enhanced Infrared Spectroscopy. *J. Am. Chem. Soc.* **2021**, *143*, 10778-10792.
- Bhattacharyya, D.; Videla, P. E.; Palasz, J. M.; Tangen, I.; Meng, J.; Kubiak, C. P.; Batista, V. S.; Lian, T. Sub-Nanometer Mapping of the Interfacial Electric Field Profile Using a Vibrational Stark Shift Ruler. *J. Am. Chem. Soc.* **2022**, *144*, 14330–14338.
- Abhayawardhana, A. D.; Sutherland, T. C. Heterogeneous Proton-Coupled Electron Transfer of an Aminoanthraquinone Self-Assembled Monolayer. *J. Phys. Chem. C* **2009**, *113*, 4915-4924.
- Nagata, M.; Kondo, M.; Suemori, Y.; Ochiai, T.; Dewa, T.; Ohtsuka, T.; Nango, M. Electron transfer of quinone self-assembled monolayers on a gold electrode. *Coll. and Surf. B: Biointerfaces* **2008**, *64*, 16-21.
- Batchelor-McAuley, C.; Kozub, B. R.; Menshykau, D.; Compton, R. G. Voltammetric Responses of Surface-Bound and Solution-Phase Anthraquinone Moieties in the Presence of Unbuffered Aqueous Media. *J. Phys. Chem. C* **2011**, *115*, 714-718.
- Forster, R. J.; O'Kelly, J. P. Protonation reactions of anthraquinone-2,7-disulphonic acid in solution and within monolayers. *J. Electroanal. Chem.* **2001**, *498*, 127-135.
- F Forster, R. J. Electron Transfer Dynamics and Surface Coverages of Binary Anthraquinone Monolayers on Mercury Microelectrodes. *Langmuir* **1995**, *11*, 2247-2255.
- Agullo, J.; Canesi, S.; Schaper, F.; Morin, M.; Bélanger, D. Formation and Reactivity of 3-Diazopyridinium Cations and Influence on Their Reductive Electrografting on Glassy Carbon. *Langmuir* **2012**, *28*, 4889-4895.

- Breton, T.; Bélanger, D. Modification of Carbon Electrode with Aryl Groups Having an Aliphatic Amine by Electrochemical Reduction of In Situ Generated Diazonium Cations. *Langmuir* **2008**, *24*, 8711-8718.
- Le Comte, A.; Chhin, D.; Gagnon, A.; Retoux, R.; Brousse, T.; Bélanger, D. Spontaneous grafting of 9,10-phenanthrenequinone on porous carbon as an active electrode material in an electrochemical capacitor in an alkaline electrolyte. *J. Mat. Chem. A* **2015**, *3*, 6146-6156.
- Toupin, M.; Bélanger, D. Spontaneous Functionalization of Carbon Black by Reaction with 4-Nitrophenyldiazonium Cations. *Langmuir* **2008**, *24*, 1910-1917.
- Weissmann, M.; Crosnier, O.; Brousse, T.; Bélanger, D. Electrochemical study of anthraquinone groups, grafted by the diazonium chemistry, in different aqueous mediarelevance for the development of aqueous hybrid electrochemical capacitor. *Electrochim. Act.* **2012**, *82*, 250-256.
- Holm, A. H.; Vase, K. H.; Winther-Jensen, B.; Pedersen, S. U.; Daasbjerg, K. Evaluation of various strategies to formation of pH responsive hydroquinone-terminated films on carbon electrodes. *Electrochim. Act.* **2007**, *53*, 1680-1688.
- Martins, M. V. A.; Pereira, A. R.; Luz, R. A. S.; Iost, R. M.; Crespilho, F. N. Evidence of short-range electron transfer of a redox enzyme on graphene oxide electrodes. *Phys. Chem. Chemical. Phys.* **2014**, *16*, 17426-17436.
- Baranton, S.; Bélanger, D. Electrochemical Derivatization of Carbon Surface by Reduction of in Situ Generated Diazonium Cations. *J. Phys. Chem. B* **2005**, *109*, 24401-24410.
- Le Comte, A.; Brousse, T.; Bélanger, D. Simpler and greener grafting method for improving the stability of anthraquinone-modified carbon electrode in alkaline media. *Electrochim. Act.* **2014**, *137*, 447-453.
- Bélanger, D.; Pinson, J. Electrografting: a powerful method for surface modification. *Chem. Soc. Rev.* **2011**, *40*, 3995-4048.
- Richard, W.; Evrard, D.; Busson, B.; Humbert, C.; Dalstein, L.; Tadjeddine, A.; Gros, P. The reduction of 4-nitrobenzene diazonium electrografted layer: An electrochemical study coupled to in situ sum-frequency generation spectroscopy. *Electrochim. Act.* **2018**, *283*, 1640-1648.
- Malka, D.; Hanna, O.; Hauser, T.; Hayne, S.; Luski, S.; Elias, Y.; Attias, R.; Brousse, T.; Aurbach, D. Improving the Capacity of Electrochemical Capacitor Electrode by Grafting 2-Aminoanthraquinone over Kynol Carbon Cloth Using Diazonium Chemistry. *J. Electrochem. Soc.* **2018**, *165*, A3342-A3349.
- Allongue, P.; Delamar, M.; Desbat, B.; Fagebaume, O.; Hitmi, R.; Pinson, J.; Saveant, J. M. Covalent modification of carbon surfaces by aryl radicals generated from the electrochemical reduction of diazonium salts. *J. Am. Chem. Soc.* **1997**, *119*, 201-207.
- Bahr, J. L.; Yang, J.; Kosynkin, D. V.; Bronikowski, M. J.; Smalley, R. E.; Tour, J. M. Functionalization of Carbon Nanotubes by Electrochemical Reduction of Aryl Diazonium Salts: A Bucky Paper Electrode. *J. Am. Chem. Soc.* **2001**, *123*, 6536-6542.
- Yates, N. D.; Dowsett, M. R.; Bentley, P.; Dickenson-Fogg, J. A.; Pratt, A.; Blanford, C. F.; Fascione, M. A.; Parkin, A. Aldehyde-Mediated Protein-to-Surface Tethering via Controlled Diazonium Electrode Functionalization Using Protected Hydroxylamines. *Langmuir* **2020**, *36*, 5654-5664.

- Baranton, S.; Bélanger, D. In situ generation of diazonium cations in organic electrolyte for electrochemical modification of electrode surface. *Electrochim. Act.* **2008**, *53*, 6961-6967.
- Yuan, W.; Zhou, Y.; Li, Y.; Li, C.; Peng, H.; Zhang, J.; Liu, Z.; Dai, L.; Shi, G. The edgeand basal-plane-specific electrochemistry of a single-layer graphene sheet.Sci. Rep. **2013**, 3, 2248.
- Sedenho, G. C.; De Porcellinis, D.; Jing, Y.; Kerr, E.; Mejia-Mendoza, L. M.; Vazquez-Mayagoitia, Á.; Aspuru-Guzik, A.; Gordon, R. G.; Crespilho, F. N.; Aziz, M. J. Effect of Molecular Structure of Quinones and Carbon Electrode Surfaces on the Interfacial Electron Transfer Process. *ACS App. Energy. Mat.* **2020**, *3*, 1933-1943.
- Anariba, F.; DuVall, S. H.; McCreery, R. L. Mono- and multilayer formation by diazonium reduction on carbon surfaces monitored with atomic force microscopy "scratching". *Anal. Chem.* **2003**, *75*, 3837-3844.
- Assresahegn, B. D.; Brousse, T.; Bélanger, D. Advances on the use of diazonium chemistry for functionalization of materials used in energy storage systems. *Carbon* **2015**, *92*, 362-381.
- Delamar, M.; Hitmi, R.; Pinson, J.; Saveant, J. M. Covalent Modification of Carbon Surfaces by Grafting of Functionalized Aryl Radicals Produced from Electrochemical Reduction of Diazonium Salts. *J. Am. Chem. Soc.* **1992**, *114*, 5883-5884.
- Yu, S.; Liu, Z.; Zhang, J.; Li, H.; Xu, N.; Yuan, X.-x.; Wu, Y. An azo-coupling reaction-based surface enhanced resonance Raman scattering approach for ultrasensitive detection of salbutamol. *RSC Adv.* **2018**, *8*, 5536-5541.
- Liu, Y. C.; McCreery, R. L. Reactions of Organic Monolayers on Carbon Surfaces Observed with Unenhanced Raman-Spectroscopy. *J. Am. Chem. Soc.* **1995**, *117*, 11254-11259.
- Kariuki, J. K.; McDermott, M. T. Formation of multilayers on glassy carbon electrodes via the reduction of diazonium salts. *Langmuir* **2001**, *17*, 5947-5951.
- 40 Rodella, C. B.; Barrett, D. H.; Moya, S. F.; Figueroa, S. J. A.; Pimenta, M. T. B.; Curvelo, A. A. S.; Teixeira Da Silva, V. Physical and chemical studies of tungsten carbide catalysts: effects of Ni promotion and sulphonated carbon. *RSC Adv.* **2015**, *5*, 23874-23885.
- Cao, D. X.; Leifert, D.; Brus, V. V.; Wong, M. S.; Phan, H.; Yurash, B.; Koch, N.; Bazan, G. C.; Nguyen, T.-Q. The importance of sulfonate to the self-doping mechanism of the water-soluble conjugated polyelectrolyte PCPDTBT-SO3K. *Mat. Chem. Front.* **2020**, *4*, 3556-3566.
- Graf, N.; Yegen, E.; Gross, T.; Lippitz, A.; Weigel, W.; Krakert, S.; Terfort, A.; Unger, W. E. S. XPS and NEXAFS studies of aliphatic and aromatic amine species on functionalized surfaces. *Surf. Sci.* **2009**, *603*, 2849-2860.
- Rabchinskii, M. K.; Ryzhkov, S. A.; Kirilenko, D. A.; Ulin, N. V.; Baidakova, M. V.; Shnitov, V. V.; Pavlov, S. I.; Chumakov, R. G.; Stolyarova, D. Y.; Besedina, N. A.; From graphene oxide towards aminated graphene: facile synthesis, its structure and electronic properties. *Sci. Rep.* **2020**, *10*.
- Ayiania, M.; Smith, M.; Hensley, A. J. R.; Scudiero, L.; McEwen, J.-S.; Garcia-Perez, M. Deconvoluting the XPS spectra for nitrogen-doped chars: An analysis from first principles. *Carbon* **2020**, *162*, 528-544.

- He, H.; Hu, Y.; Chen, S.; Zhuang, L.; Ma, B.; Wu, Q. Preparation and Properties of A Hyperbranch-Structured Polyamine adsorbent for Carbon Dioxide Capture. *Sci. Rep.* **2017**, 7
- Bogdanowicz, R.; Sawczak, M.; Niedzialkowski, P.; Zieba, P.; Finke, B.; Ryl, J.; Karczewski, J.; Ossowski, T. Novel Functionalization of Boron-Doped Diamond by Microwave Pulsed-Plasma Polymerized Allylamine Film. J. Phys. Chem. C 2014, 118, 8014-8025.
- 47 Yang, X.; Wu, Z.; Sun, L.; Ni, C. The bromination mechanism of 1-aminoanthraquinone-2,4-disulfonic acid in sulfuric acid. *Dyes and Pig.* **2006**, *71*, 231-235.
- 48 Artemenko, A.; Shchukarev, A.; Štenclová, P.; Wågberg, T.; Segervald, J.; Jia, X.; Kromka, A. Reference XPS spectra of amino acids. *IOP Conf. Series: Mat. Sci. and Eng.* **2021**, *1050*, 012001.
- Silva, K.; Marco, J. F.; Yañez, C. Covalent Immobilization of Amino-β-Cyclodextrins on Glassy Carbon Electrode in Aqueous Media. *J. Electrochem. Soc.* **2019**, *166*, G75-G81.
- Huskinson, B., Marshak, M. P., Suh, C., Er, S., Gerhardt, M. R., Galvin, C. J., Chen, X., Aspuru-Guzik, A., Gordon, R. G., Aziz, M. J. A metal-free organic-inorganic aqueous flow battery. *Nature* **2014**, *505*, 195-198.
- Turcanu, A.; Bechtold, T. pH Dependent redox behaviour of Alizarin Red S (1,2-dihydroxy-9,10-anthraquinone-3-sulfonate) Cyclic voltammetry in presence of dispersed vat dye. *Dyes and Pig.* **2011**, *91*, 324-331.
- Amiri, M.; Shul, G.; Donzel, N.; Bélanger, D. Aqueous electrochemical energy storage system based on phenanthroline- and anthraquinone-modified carbon electrodes. *Electrochim. Act.* **2021**, *390*, 138862.
- 53 Smith, C. P.; White, H. S. Theory of the interfacial potential distribution and reversible voltammetric response of electrodes coated with electroactive molecular films. *Anal. Chem.* **1992**, *64*, 2398-2405.
- Costentin, C. Electrochemical approach to the mechanistic study of proton-coupled electron transfer. *Chem. Rev.* **2008**, *108*, 2145-2179.
- Jackson, M. N.; Pegis, M. L.; Surendranath, Y. Graphite-Conjugated Acids Reveal a Molecular Framework for Proton-Coupled Electron Transfer at Electrode Surfaces. *ACS Cent. Sci.* **2019**, *5*, 831-841.
- Guthrie, J. P. Hydrolysis of esters of oxy acids: pKa values for strong acids; Brønsted relationship for attack of water at methyl; free energies of hydrolysis of esters of oxy acids; and a linear relationship between free energy of hydrolysis and pKa holding over a range of 20 pK units. *Can. J. Chem.* **1978**, *56*, 2342-2354.
- Zebardast, H. R., Rogak, S. & Asselin, E. Potential of zero charge of glassy carbon at elevated temperatures. *J. Electroanal. Chem.* **2014**, *724*, 36-42.
- Rahimi, M.; Catalini, G.; Hariharan, S.; Wang, M.; Puccini, M.; Hatton, T. A. Carbon Dioxide Capture Using an Electrochemically Driven Proton Concentration Process. *Cell Rep. Phy. Sci.* **2020**, *1*, 100033.
- Rahimi, M.; Catalini, G.; Puccini, M.; Hatton, T. A. Bench-scale demonstration of CO2 capture with an electrochemically driven proton concentration process. *RSC Adv.* **2020**, *10*, 16832-16843.
- Jin, S.; Wu, M.; Gordon, R. G.; Aziz, M. J.; Kwabi, D. G. pH swing cycle for CO2 capture electrochemically driven through proton-coupled electron transfer. *Energy & Env. Sci.* **2020**, *13*, 3706-3722.

- Schmickler, W. Electronic Effects in the Electric Double Layer. *Chem. Rev.* **1996**, *96*, 3177-3200.
- Tarpeh, W. A.; Barazesh, J. M.; Cath, T. Y.; Nelson, K. L. Electrochemical Stripping to Recover Nitrogen from Source-Separated Urine. *Env. Sci. & Tech.* **2018**, *52*, 1453-1460.
- Favaro, M.; Jeong, B.; Ross, P. N.; Yano, J.; Hussain, Z.; Liu, Z.; Crumlin, E. J. Unravelling the electrochemical double layer by direct probing of the solid/liquid interface. *Nat. Comm.* **2016**, *7*, 12695.
- Zoric, M. R.; Askins, E. J.; Qiao, X.; Glusac, K. D. Strong Electronic Coupling of Graphene Nanoribbons onto Basal Plane of a Glassy Carbon Electrode. *ACS App. Elect. Mat.* **2021**, *3*, 854-860.
- Zhou, W.; Kolb, D. M. Influence of an electrostatic potential at the metal/electrolyte interface on the electron binding energy of adsorbates as probed by X-ray photoelectron spectroscopy. *Surf. Sci.* **2004**, *573*, 176-182.

TOC Graphic

